

# Periodic orbits in plane Couette flow

Tobias Kreilos

*Fachbereich Physik, Philipps-Universität Marburg, D-35032 Marburg, Germany*

Bruno Eckhardt

*Fachbereich Physik, Philipps-Universität Marburg, D-35032 Marburg, Germany and  
J.M. Burgerscentrum, Delft University of Technology, Mekelweg 2, 2628 CD Delft, The Netherlands*

(Dated: October 6, 2022)

We track the secondary bifurcations of coherent states in plane Couette flow and show that they undergo an incomplete periodic doubling cascade that ends with a crisis bifurcation. We introduce a symbolic dynamics for the orbits and show that the ones that exist fall into the universal sequence described by Metropolis, Stein and Stein for unimodal maps. The periodic orbits cover much of the turbulent dynamics in that their temporal evolution overlaps with turbulent motions when projected onto a plane spanned by energy production and dissipation.

The identification of the different ‘routes to chaos’ [1, 2] has suggested ways in which they can also be ‘routes to turbulence’ that lead from a laminar flow state through various bifurcations to a turbulent attractor. Studies of the turbulence transition in plane Couette flow and pipe flow, which do not have a linear instability of the laminar profile, have revealed a route to turbulence that passes through the formation of a chaotic saddle [3, 4]. The saddle develops around a scaffold of coherent structures that appear in saddle-node type bifurcations, with the notable difference to the standard scenario that also the ‘node’-states are typically unstable. In this transitional region the turbulence is not persistent but transient, and can hence be associated with a transient chaotic saddle rather than an attractor. In the spirit of a dynamical systems approach to characterizing these features [5], we here present an analysis of the phase space structures near transition in plane Couette flow and study the various bifurcations and periodic orbits that appear.

## I. INTRODUCTION

The application of dynamical systems ideas to fluid mechanical problems has provided much insight into the ways fluids transit from a laminar state to a turbulent one. The various bifurcations that appear in the case of fluids heated from below (Rayleigh-Benard) or fluids driven by centrifugal instabilities (Taylor-Couette) have been studied experimentally and theoretically in considerable detail [6, 7]. Studies of turbulence in liquid helium have shown the period doubling cascade [8] and the quasi-periodic routes to chaos [9], and the rich structures of secondary bifurcations and flow states in RB and TC have been explored [6, 7, 10]. The approach has been so successful that flows without linear stability of the linear profile, like plane Couette flow and pipe flow, have been

suspected to belong to the class of subcritical bifurcations [11], perhaps with the bifurcation point at infinity (as reflected, e.g., in the title of Nagata’s first papers on coherent structures in pipe flow [12]). However, the first structures that are observed near the transition point are not steady or simple flows, but they are fluctuating spatially and temporally, indicating that these states undergo many further bifurcations as the Reynolds number is lowered.

A more promising approach starts with the turning points of the subcritical bifurcations, the saddle-node bifurcations in which these structures appear. The possibility to approach flows from this point of view is suggested by the remarkable persistence of key features of these structures [3]: they are all dominated by downstream vortices which modify the base profile to generate streaks. This by itself is not enough, as flows that are translationally invariant in the downstream direction cannot be sustained [13]. So three-dimensionality is another key element, and also the reason for the absence of analytical studies of this transition scenario.

The importance of vortices and streaks has been deduced from numerical studies of plane Couette flow in small domains, where a recurrent pattern of vortices and streaks could be identified [14, 15]. The interactions between vortices and streaks and the instabilities that streaks can undergo has been studied by Waleffe [16], who proposed a self-sustaining cycle (analyzed also in [17–20]). The cycle is usually explained by starting with the vortices, which then drive streaks, and the streaks then undergo an instability in which normal vorticity is created. To close the cycle, this normal vorticity is then argued to be turned into downstream vorticity by the mean profile.

An example where the transitions between the different states and their symmetry can be analyzed directly, and in a physically meaningful setting, is Taylor-Couette flow in the limit in which it approaches plane Couette flow [21]. In the curved case, say with the inner cylinder rotating and the outer one at rest, the flow undergoes a first bifurcation to Taylor-vortex flow, in which vortices with an azimuthal symmetry appear. As the rotation

rate is increased, the vortices undergo a secondary bifurcation, in which an azimuthal modulation is added and the rotational symmetry is broken. Increasing the radii while keeping the distance between the cylinders fixed, the influence of the curvature becomes smaller and the flow approaches plane Couette flow. Along the way, the bifurcation structure changes: the transition point to the formation of azimuthally symmetric vortices moves out infinity, so that the linear stability of plane Couette flow is recovered. The three-dimensional wave structures, however, can be traced over to plane Couette flow, where they now appear in a saddle node bifurcation [21]. In going from the Taylor-Couette to plane-Couette flow the transition can be studied within realistic models. In the case of pipe flow no physical family of flows could be identified, so a body force was introduced to embed the system into one where the bifurcations can be realized. Despite this artificial setting, the coherent structures thus found are similar to the ones in plane Couette flow and share many properties [22].

The coherent structures just described are usually unstable, and can appear only transiently in the flow [23–25]. Moreover, it was found that they are not sufficiently entangled to close off the phase space around them to form an attractor: thus it is not only the coherent structures that are visited transiently, but the entire turbulent dynamics becomes a transient phenomenon, characterized by an exponential distribution of lifetimes, as can be expected for a chaotic saddle [26, 27]. While this sets the stage from the dynamical systems point of view, a couple of questions remain to be addressed [4]. We will address two of them, related to the secondary bifurcations of coherent structures, in the following.

It was noticed long ago in [28], that the coherent structures that appear in plane Couette flow at  $Re = 125$  are stable very close to the bifurcation point and become unstable via Hopf bifurcations. This would suggest that the transition creates an attractor rather than a transient saddle. However, at higher  $Re$  the flow is evidently transient: so how does the phase space near these coherent states change as one increases the Reynolds number and how does the flow change from chaotic but persistent to transient? The analysis of these properties in pipe flow shows that the sequence of bifurcations that lead from a (small) chaotic attractor to transient dynamics can be rather intricate [29, 30].

A second item concerns the possibility to describe the flows using periodic orbits, as is possible in other dynamical systems [5, 31, 32]. Identifying periodic orbits in high-dimensional systems is a major technical challenge, which has been overcome in a few cases only. Most notably, for the cases studied here, a few isolated periodic orbits have been found in [33]. In the present case their identification is considerably simplified by the presence of a period doubling cascade.

The outline of the paper is as follows: in section II we discuss the organization of the phase space near the lowest saddle-node bifurcation in plane Couette flow. In

section III we discuss the characterization of the internal dynamics and bifurcations in terms of a discrete map. We follow this in section IV with a discussion of the periodic orbits and their properties.

## II. BIFURCATIONS

We study an incompressible Newtonian fluid between two infinitely extended plates in the  $x$ - $z$  plane located at  $y = \pm h$  that move with speed  $\pm U_0$  along the  $x$ -axis. A length-, velocity and time-scale are given by  $h$ ,  $U_0$  and  $t = h/U_0$ . The control parameter is the Reynolds number  $Re = U_0 d/\nu$ , where  $\nu$  is the viscosity of the fluid. We use periodic boundary conditions in the spatially extended directions and no-slip boundary conditions at the walls, with a box size of  $2\pi \times 2 \times \pi$  in the downstream, wall-normal and spanwise directions, respectively. We use *channelflow* [34] to integrate this system with a Fourier-Chebyshev-Fourier scheme and a numerical resolution of  $32 \times 33 \times 32$  modes. The main quantity we use in this study is the cross-flow energy, i.e. the amount of energy in the flow components transverse to the laminar base flow,

$$E_{cf} = \frac{1}{V} \int_V (v^2 + w^2) dV, \quad (1)$$

or the square root of  $E_{cf}$  so as to reduce the range of it.

The box size in this study is just slightly longer and narrower than the cell studied in Ref. [15]. In this and other smaller boxes the typical flow consists of a pair of counter-rotating streamwise vortices and a pair of alternating streaks. This limitation in the number of possible flow structures greatly simplifies the sequence of bifurcations. To simplify the analysis even further we enforce a shift-and-reflect symmetry

$$\sigma[u, v, w](x, y, z) = [u, v, -w](x + L_x/2, y, -z), \quad (2)$$

which, up to a discrete displacement by  $L_z/2$ , fixes the spanwise location of the flow structures.

The different box size compared to the calculations by Nagata [12] and Clever and Busse [28] has the effect of moving the first bifurcation to a higher Reynolds number, namely  $Re = 163.8$ , where a pair of fixed points appears in a saddle-node bifurcation. The lower branch equilibrium (LB) has one unstable direction, the upper branch equilibrium (UB) is linearly stable. Since the laminar profile is linearly stable for all Reynolds numbers [35], there now coexist two attractors. The separatrix of their basins of attraction is formed by the stable manifold of LB.

The situation is illustrated in figure 1(a). The initial conditions that correspond to the points in the plane of the figures are spanned by the laminar profile, and the upper and lower branch states. The  $x$ -axis is a linear interpolation between LB and UB and the  $y$ -axis gives the

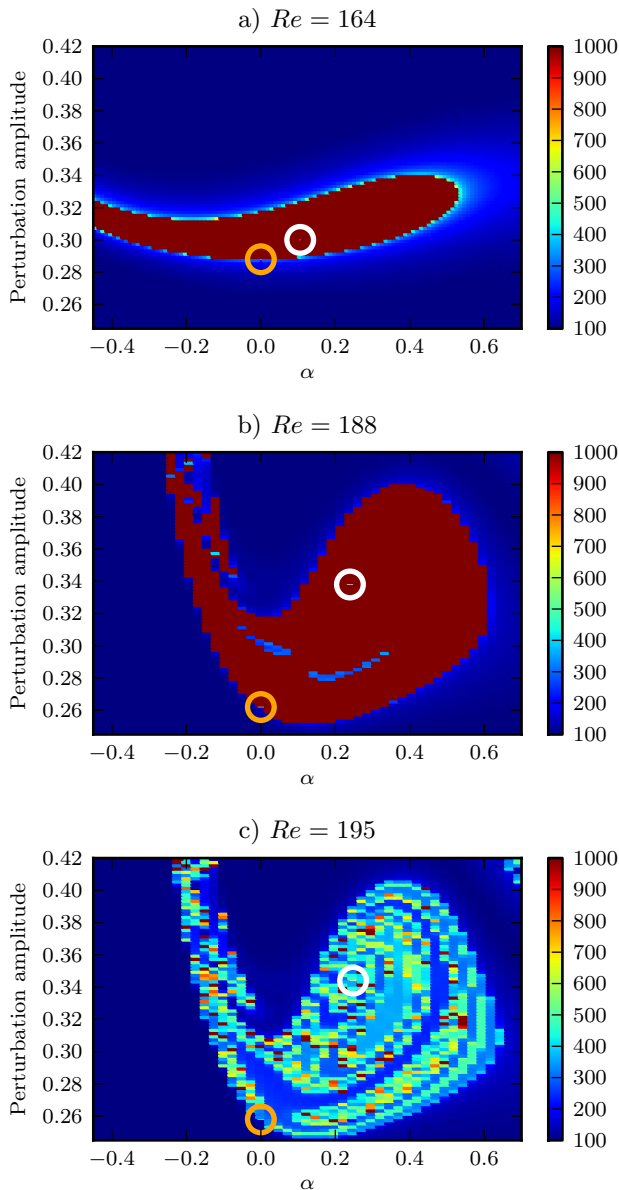


FIG. 1. The basins of attraction of the attractors in plane Couette flow for three Reynolds numbers near the bifurcation point of the Nagata-Clever-Busse-state. Basins are depicted by the lifetime of initial conditions. States on the  $x$ -axis are obtained by interpolating between the lower- and the upper-branch solution, rescaled by a factor that ensures that the distance between the two solutions in the plot is equal to the  $L_2$ -norm of their difference, see equation (4). These states are then scaled in amplitude along the  $y$ -axis. The lower branch equilibrium is marked with an orange circle, the upper one with a black circle. (a) For  $Re$  just slightly above the bifurcation point, the basin of attraction of the upper branch is a small region with a bubble-like shape. Its boundary is formed by the stable manifold of the lower branch. (b) For  $Re = 188$ , the overall structure has not changed a lot, though the attractor is no longer a fixed point but a chaotic orbit. (c) At  $Re = 188.51$  a boundary crisis occurs – the chaotic attractor becomes “leaky” and all trajectories eventually relaminarize. This bubble-like shape remains visible as an envelope of the initial conditions for longer living states, though.

perturbation amplitude with which the state is scaled. Formally, the initial conditions are given by

$$u(\alpha, A) = A \cdot u_\alpha / \|u_\alpha\| \quad (3)$$

with

$$u_\alpha = u_{LB} + \frac{\alpha \cdot (u_{UB} - u_{LB})}{\sqrt{\|u_{UB} - u_{LB}\|^2 - (\|u_{UB}\| - \|u_{LB}\|)^2}}. \quad (4)$$

The division by the root scales the  $x$ -axis in a way that the distance between LB and UB in the plot corresponds to the  $L_2$ -norm of the difference between the two fixed points.

The basins of attraction are obtained by studying the lifetimes, defined as the time it takes for the flow to satisfy for the first time the condition  $E_{cf}(u(t) - u_{lam}) < \epsilon = 10^{-8}$ . Initially, when the basin of attraction is closed and trajectories are attracted to a stable fixed point that is not the laminar profile, there is a solid block of long, actually infinite, lifetimes. The stable fixed point lies somewhere in the center of the blob and the unstable saddle lies on its boundary.

A notable feature of these plots is the bubble shape of the basins of attraction of the stable fixed points. The unstable manifold of the unstable fixed point that loops around the stable fixed point folds back to approach the other branch of the stable manifold. This behaviour was identified by Lebovitz [36, 37] in a model flow, and as the present figures shows it also is relevant to full representations of the flow. In view of the bifurcation structures described in [29] one can expect that this bubble shape is rather generic.

As Reynolds number increases, the stability properties of LB do not change up to at least  $Re = 400$ . On the other side, UB is only an attractor for a very short range and undergoes a Hopf bifurcation at  $Re_H = 166.05$ , which has already been noted by Clever and Busse [28]. The bifurcation is supercritical, as is revealed by the emergence of a limit cycle whose amplitude grows as  $\sqrt{Re - Re_H}$ . The emerging stable periodic orbit undergoes a period doubling at  $Re = 178.9$  which, for this domain size, results in an incomplete period doubling cascade.

While the way to represent fixed points in a bifurcation diagram is straightforward, it is less so for periodic orbits or chaotic trajectories. To visualize the attracting state once it gets more complicated we introduce a reduced representation of the flow by focussing on the maxima in energy: we calculate a typical trajectory originating near UB (and hence not lying in the basin of attraction of the laminar state), omit an initial transient and all intermediate times except for the maxima. We then keep values of the maxima in  $\sqrt{E_{cf}}$  to represent the flow. The method is illustrated in figure 2, where a short section of a typical chaotic trajectory for  $Re = 187.8$  is shown. The maxima are marked with symbols corresponding to the symbolic dynamics that will be introduced in section III.

The bifurcation cascade is summarized in figure 3, where the square root of the cross-flow energy  $E_{cf}$  is

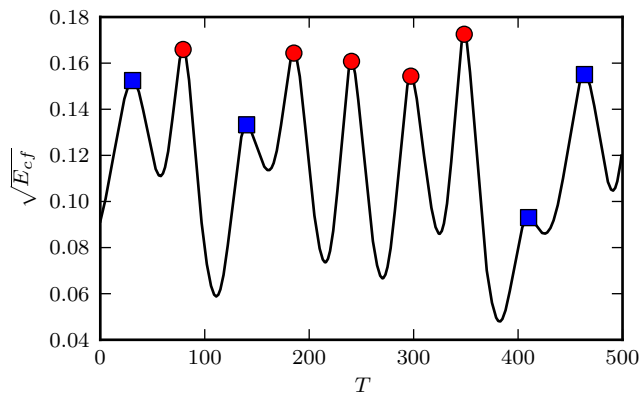


FIG. 2. Example of a typical chaotic trajectory at  $Re = 187.8$ . For the reduction to a map, we only keep the energies at the maxima. The different symbols assigned to the maxima follow from the symbolic dynamics that will be introduced in section III: squares represent the symbol "0" and circles the symbol "1".

plotted. The attractor is plotted with a dot for every maximum of  $E_{cf}$ , LB is a dashed line and UB is a dotted line once it becomes unstable. In this representation the emergence of a limit cycle at  $Re_H$  with an amplitude that grows as  $\sqrt{Re - Re_H}$  is clearly visible. It is followed by a period doubling cascade resulting in a chaotic attractor. We find a stable period three window from  $Re = 183.8$  to  $Re = 185.0$ , followed by a new period doubling cascade of the period three orbit. The basin of attraction is still confined to a small region in state space, as is evident from figure 1(b), which shows the basin for  $Re = 188$ . Compared to the above picture at  $Re = 164$ , the general shape of the basin has not changed. Near the crisis bifurcation perhaps also the homoclinic tangles described in [38] form. The transition in the lifetimes is in agreement with the phenomenology observed also in the two-dimensional map described in [39].

For  $Re > Re_c = 188.51$ , there are no more dots in figure 3: all trajectories eventually relaminarize. Our interpretation is that at  $Re_c$  the chaotic attractor touches the fixed point LB (or, equivalently, its stable manifold) and a boundary crisis [40] occurs and the attractor becomes "leaky". Even though the crisis is not visible in figure 3 due to the chosen representation, it will become visible later in another view of state space, see figures 11 below. We show a phase space plot of  $Re = 195$  in figure 1(c). The bubble shape that formed the basin of attraction of the chaotic attractor before the crisis is still visible. But the lifetimes of the initial conditions from that region now are no longer infinite but vary drastically between almost direct decay and very long survival. The distribution of the lifetimes (not shown here) turns out to be exponential – a signature of a chaotic saddle left behind by the boundary crisis [25].

### III. SYMBOLIC DYNAMICS

In this and the next section we focus on the situation just before the crisis, namely at  $Re = 187.8$ , where the attractor is chaotic. We now use the reduction of the flow to the location of its maxima to introduce an approximately one-dimensional map of the flow. We denote the value of the  $i$ -th maximum of  $\sqrt{E_{cf}}$  along this trajectory by  $x_i$  and plot  $x_{i+1}$  vs.  $x_i$ . This then gives a reduced, approximate map  $x_i \rightarrow x_{i+1} = f(x_i)$ . Figure 4 shows a plot of the map obtained from a trajectory with 10798 maxima.

In this representation, the attractor looks very thin and almost one-dimensional, though a fractal structure can be seen perpendicular to it. In this sense it is qualitatively similar to fractal attractors in well-known low-dimensional systems like the Hénon map with standard parameters. The attractor consists of several branches, all of which show a distinctive maximum between  $x_i = 0.14$  and  $x_i = 0.16$ , but the location of the maxima do not coincide.

Given this representation of the attractor, we introduce a binary symbolic dynamics in the usual way: on each branch, a point is labeled as 0 or 1 if it lies to the left or right of the maximum, respectively. The symbolic dynamics is shown in figure 5 for the same snapshot of the trajectory as in figure 2. We find that a partition cannot be based on a single value of  $x_i$  and that the branch on which it comes to lie also has to be taken into account:  $x_6$  is a little lower than  $x_9$  but assigned the symbol "1" while  $x_9$  is assigned "0" because of its different location relative to the maximum of the corresponding branch. The two rightmost squares in figure 5(b) lie on the branch of the rightmost maximum while the circle just above them lies on the branch of a maximum further left.

### IV. PERIODIC ORBITS

In this section, we will describe the periodic orbits we found at  $Re = 187.8$ . We obtain initial guesses by scanning the map  $f$  (figure 4) for close returns along a trajectory and then use channelflows excellent Newton-Krylov-Hookstep algorithm [41] for finding periodic orbits. Since the attractor for this Reynolds number is chaotic, we expect all orbits to be linearly unstable. For reasons of computational stability we restrict the search to orbits of symbolic period not exceeding five.

With this method we found seven different orbits – they are listed, along with their properties in table I. The first column contains the symbolic name of the orbit, the second one the period of the orbit in time-units of Navier-Stokes. The Reynolds number where the orbits bifurcate, either pitchfork or saddle node bifurcations, are given in the fourth column. The orbit  $\bar{1}$  is created in a Hopf-bifurcation of UB, the orbits  $\bar{0}\bar{1}$  and  $\bar{0}\bar{1}\bar{1}$  result from period-doublings of the former one. The pairs of the two period-3 and period-5 orbits are the re-

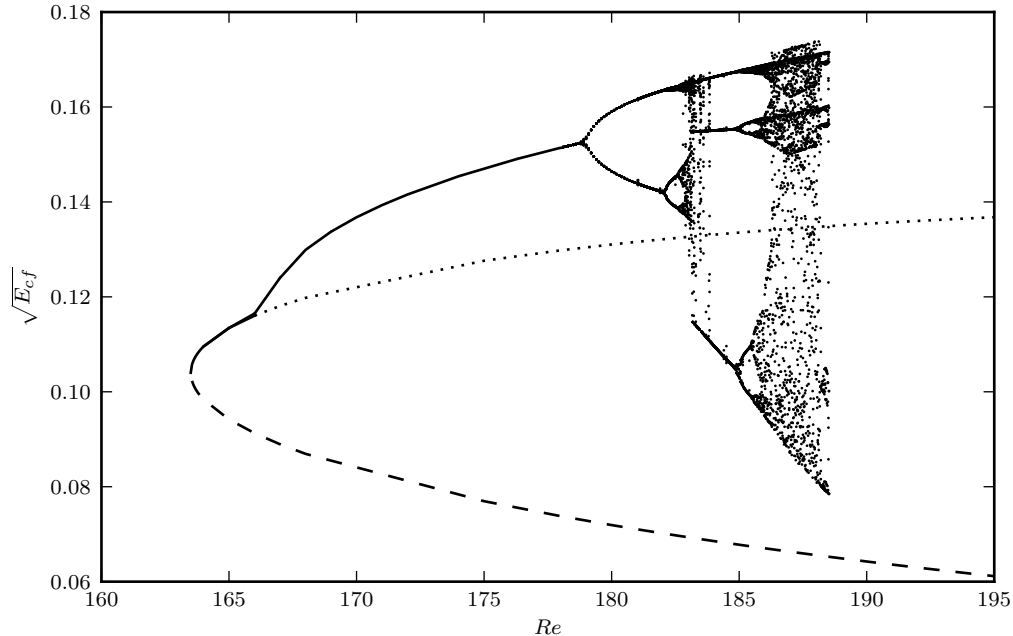


FIG. 3. The square root of the kinetic energy  $\sqrt{E_{cf}}$  for the upper- and lower-branch solutions and the attractor coexisting with the laminar state. To visualize periodic orbits and chaotic attractors, we plot every maximum of  $E_{cf}$  with a dot. The Nagata-Clever-Busse-state is born in a saddle-node bifurcation at  $Re = 163.8$ , we plot the lower branch with a dashed line and the upper branch with a line as long as it is stable and with a dotted line afterwards. The upper branch loses stability in a Hopf bifurcation at  $Re = 166.05$ , the emergence of a limit cycle is nicely visible. It undergoes a period doubling cascade. After the boundary crisis at  $Re = 188.51$ , no second attractor exists beneath the laminar state.

Orbit	$T$	$Re_{Bif}$	$\Lambda_1$	$\lambda_1$	$\Lambda_2 - 1$	$\Lambda_3 - 1$	$\Lambda_4$	$\lambda_4$
$\bar{1}$	55.22	166.0	-2.64	0.0176	$9.83 \cdot 10^{-7}$	$-5.65 \cdot 10^{-7}$	0.4	-0.0166
$\overline{01}$	106.95	172.3	-4.79	0.0146	$2.11 \cdot 10^{-6}$	$-5.33 \cdot 10^{-7}$	0.13	-0.0191
$\overline{001}$	162.1	181.9	-4.6	0.0094	$1.95 \cdot 10^{-5}$	$2.76 \cdot 10^{-6}$	0.05	-0.0185
$\overline{011}$	159.21	181.9	9.43	0.0141	$1.37 \cdot 10^{-7}$	$-4.33 \cdot 10^{-6}$	0.048	-0.0191
$\overline{0111}$	215.84	182.1	-27.73	0.0154	$3.56 \cdot 10^{-4}$	$-8.81 \cdot 10^{-7}$	0.017	-0.0189
$\overline{01101}$	266.87	182.2	-50.67	0.0147	$4.21 \cdot 10^{-3}$	$-1.70 \cdot 10^{-5}$	0.0063	-0.0190
$\overline{01111}$	270.65	182.2	76.63	0.0160	$4.87 \cdot 10^{-6}$	$4.87 \cdot 10^{-6}$	0.0061	-0.0188

TABLE I. Properties of the periodic orbits. The first column contains the symbolic sequence of the orbit, the second column the period in time-units of Navier-Stokes. The fourth column gives the Reynolds numbers where the orbits are created. The last four columns give the eigenvalues with the largest magnitudes. All orbits have one and only one unstable eigenvalue.

sult of saddle-node bifurcations. To better illustrate the bifurcation sequence, we show the bifurcation diagram again in figure 6 with the bifurcation points indicated by dashed lines. The solid line at  $Re = 187.8$  indicates the Reynolds number where the analysis of the symbolic dynamics takes place.

The bifurcation sequence of the orbits is almost the same as the universal sequence described by Metropolis, Stein and Stein [42], with the only exception being that the period-doubling of  $\overline{01}$  that creates  $\overline{0111}$  takes place slightly after the saddle-node bifurcations in which the orbits  $\overline{001}$  and  $\overline{011}$  appear. We have not found the orbits

$\overline{0011}$ ,  $\overline{0001}$ ,  $\overline{00111}$ ,  $\overline{00011}$ ,  $\overline{00001}$  and  $\overline{00101}$  – which is in accordance with the universal sequence for an incomplete cascade.

The eigenvalues  $\Lambda_i$  of the monodromy matrix of the periodic orbits are calculated using Arnoldi iteration [41]. From the eigenvalues  $\Lambda_i$  one can extract Lyapunov exponents  $\lambda_i = \ln |\Lambda_i|/T$ . The four eigenvalues of largest magnitude and the corresponding nontrivial Lyapunov exponents are given in the last six columns of table I. All of the periodic orbits have exactly one unstable eigenvalue  $\Lambda_1$  and two eigenvalues  $\Lambda_{2,3}$  that correspond to translation along  $x$  and time that are theoretically strictly equal

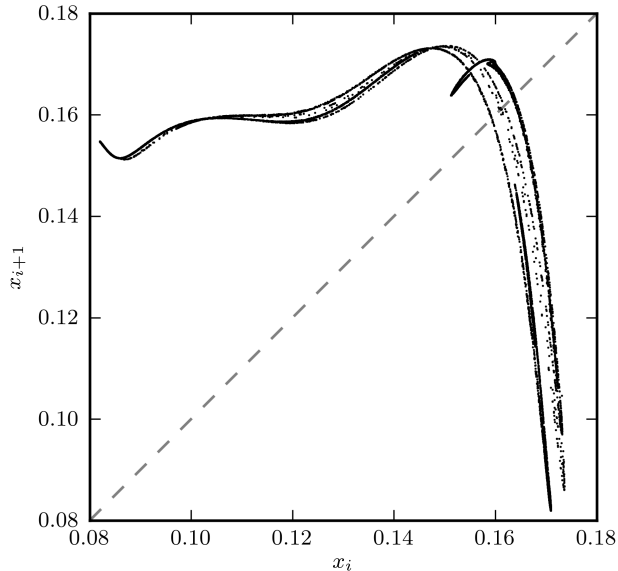


FIG. 4. The chaotic attractor at  $Re = 187.8$ . It is obtained by calculating for a trajectory that contains 10799 maxima of  $E_{cf}$ . The values of the maxima of  $\sqrt{E_{cf}}$  are denoted  $x_i$  for the  $i$ -th maximum and the map is obtained by plotting  $x_{i+1}$  vs.  $x_i$ . It consists of several branches that lie close to each other and, for the purposes of labelling trajectories, can be collapsed into a one-dimensional uni-modal map. A binary symbolic dynamics can be introduced according to the relative location of the points: points that lie on a branch left or right of the maximum are labeled 0 or 1, respectively.

to 1 (translations along  $z$  are excluded by the enforced shift-and-reflect symmetry). The deviation of  $\Lambda_{2,3}$  from 1 can be used as a measure of the accuracy of our numerics.  $\Lambda_4$  is the least stable eigenvalue of the orbit and measures the contraction in the directions perpendicular to the attractor. The positive first Lyapunov exponent varies between 0.0094 and 0.176, where the largest value comes from the shortest orbit  $\bar{1}$ . All orbits have exactly one unstable direction and their weakest contracting Lyapunov exponent  $\lambda_4$  is of the same order, this supports the conjecture that the system can be approximated by a one dimensional map.

The upper branch becomes unstable via a Hopf bifurcation and at  $Re = 187.8$  the complex conjugate pair of eigenvalues is still the only unstable ones. The values are  $\lambda_{1,2} = 0.023 \pm 0.128$  and the imaginary part corresponds to a period of  $T = 2\pi/\Im(\lambda) = 48.93$  which is not too far from the period of the orbit  $\bar{1}$ .

The orbit  $\bar{0}$  is missing in table I. An estimate of what its properties could be can be calculated from the  $\bar{1}$  and the longer orbits in the following way: let  $n_0$  the number of zeros in the symbolic sequence and  $n_1$  the number of ones. Then an estimate for the time-period of  $\bar{0}$  is obtained from an orbit composed of  $n_0$  and  $n_1$  symbols "0" and "1", respectively, can be obtained as follows: Since the

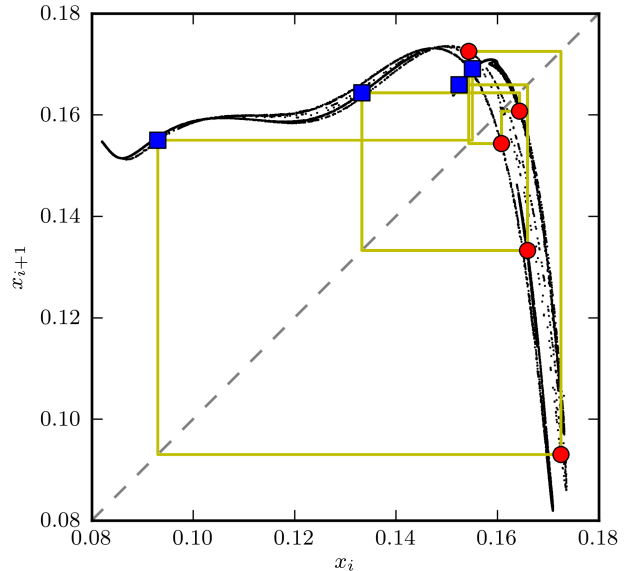


FIG. 5. Symbolic dynamics for the same trajectory as in figure 2, squares are 0 and circles 1. The rightmost square is left of the maximum and has to be labeled as 0 despite the fact that it is further right than the leftmost circle.

Orbit	$T(\bar{0})_{Est}$	$\lambda_1(\bar{0})_{Est}$	$\lambda_4(\bar{0})_{Est}$
$\bar{01}$	51.73	0.0115	-0.0217
$\bar{001}$	53.44	0.0052	-0.0195
$\bar{011}$	48.77	0.0062	-0.0247
$\bar{0111}$	50.18	0.0082	-0.0264
$\bar{01101}$	50.61	0.0100	-0.0229
$\bar{01111}$	49.77	0.0092	-0.0288

TABLE II. Estimates of some properties of the missing orbit  $\bar{0}$ , calculated from the longer orbits. See text for details.

properties of the long orbit are similar to a superposition of  $n_0$  and  $n_1$  shorter segments, we can estimate the time from

$$T_0^{est} \approx (T - n_1 T(\bar{1}))/n_0 \quad (5)$$

, and the Lyapunov exponent from

$$\lambda_0^{est} \approx (\lambda T - n_1 \lambda_1 T_1)/n_0 T_0 \quad (6)$$

they are given in table II. All estimates indicate that the time-period of  $\bar{0}$  would be slightly shorter than that of  $\bar{1}$ . While estimations for the first Lyapunov exponent  $\lambda_1$  fluctuate by more than a factor of two, reflecting the fluctuations in the stability of the orbits themselves, the least stable exponent fluctuates less; it is slightly more contracting than those of the other orbits.

Cobweb-plots of all orbits are presented in figure 7. While most of the orbits concentrate in the upper right

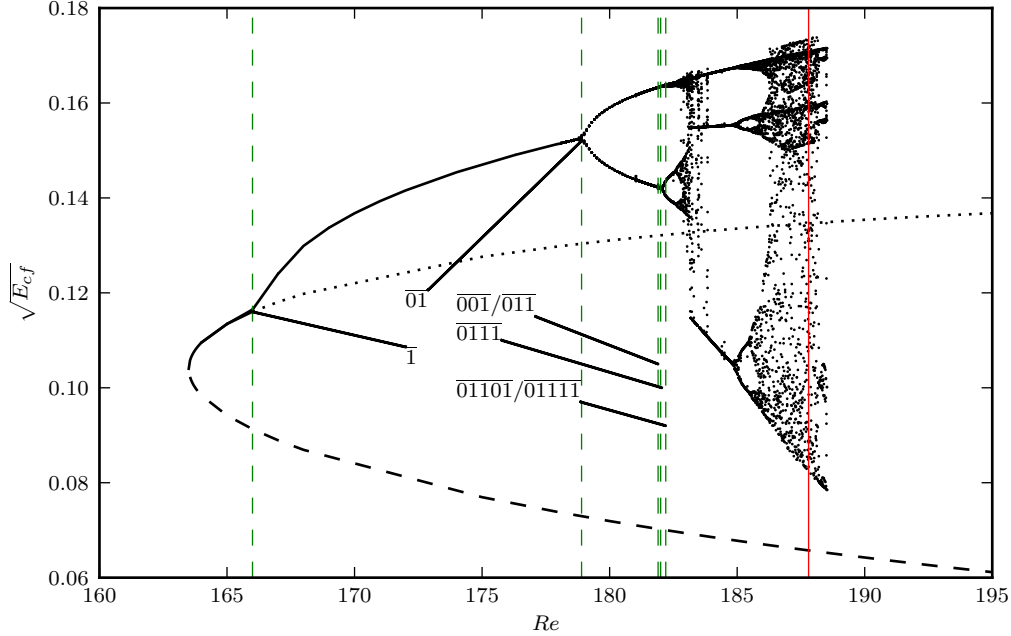


FIG. 6. Critical Reynolds numbers for the periodic orbit bifurcations, indicated with dashed lines. The straight line at  $Re = 187.8$  corresponds to the Reynolds number where the analysis takes place.

corner of the map, only  $\overline{001}$  stretches out to the lowest and highest values. Since  $\overline{001}$  is the only orbit with a sequence 00, this suggests that longer orbits containing 00 would also stretch out to those more extreme regions of the attractor.

In figures 8 and 9 we present orbits in a plane spanned by the cross-flow energy  $E_{cf}$  and the friction factor  $C_f$ , respectively. Figure 8 shows nicely the composition of the longer orbits as repetitions of the shorter ones. For example, the orbit  $\overline{011}$  is very similar to  $\overline{0111}$  and  $\overline{01111}$ , except that the latter ones have one (two) additional peak(s) that looks quite similar to  $\overline{1}$ . Note also how the orbits explore the ranges covered by a turbulent trajectory, lending support to the idea that periodic orbits can be used to represent all possible motions and that averages could be calculated from the periodic orbits.

We show some averaged quantities of the orbits in figure 10. We use small letters for the fluctuating components and  $U_0$  for the base flow. The left plot shows  $\langle u \rangle + U_0$ , the middle one  $\langle uu \rangle$  and the right one  $\langle vv \rangle$ . In all three plots, the mean profiles for nearly all orbits impossible to distinguish among each other. Within the group of orbits of period less than six, the exception is  $\overline{001}$ , which is marginally offset to the right in (b) and (c). We indicate the averages obtained from a chaotic trajectory with 5000 time units by crosses – they can hardly be distinguished from the averages of the periodic orbits.

The motion of the walls injects energy into the fluid motion which in turn is dissipated by viscosity. The en-

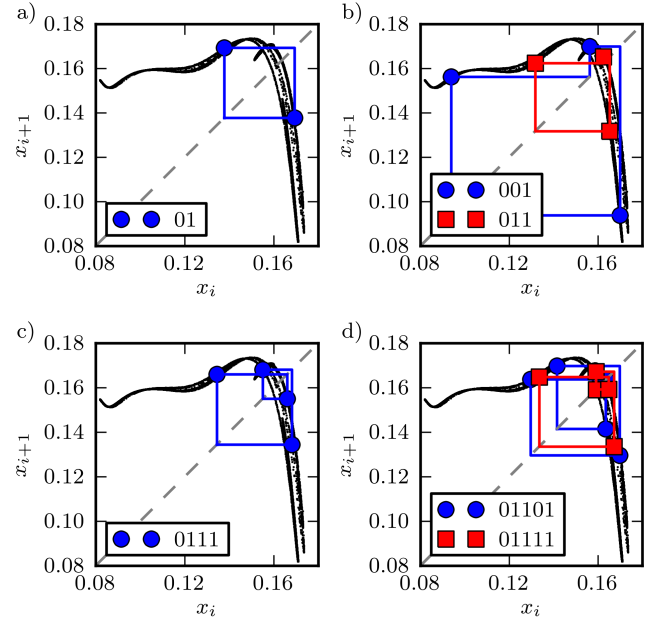


FIG. 7. The periodic orbits, presented in cobweb-plots. Only the orbit  $\overline{001}$  visits the extremest position on the attractor.

ergy balance can be written as [43]

$$\dot{E} = I - D,$$



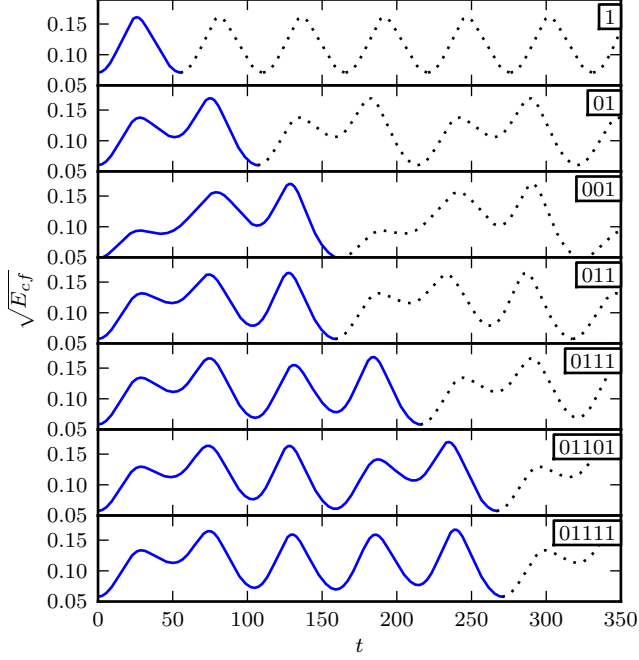


FIG. 8. The root of the cross-flow energy  $\sqrt{E_{cf}}$  for all periodic orbits. The composition of the longer orbits from parts of the shorter ones is nicely visible.

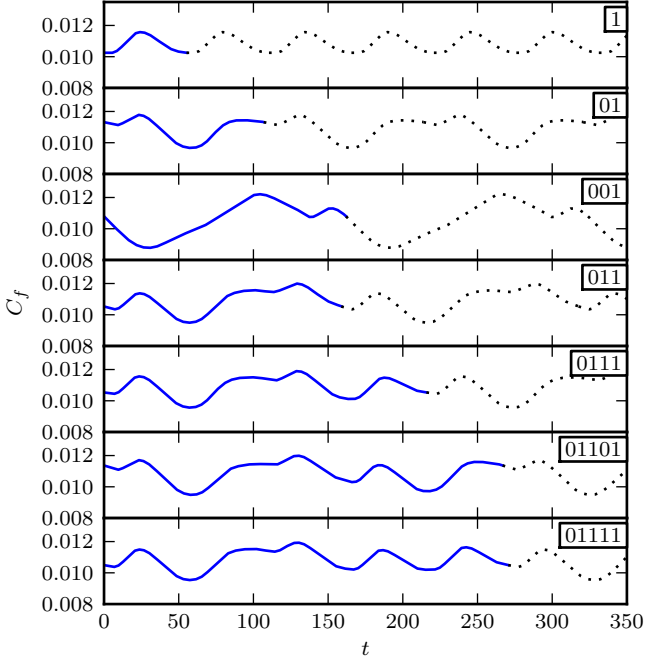


FIG. 9. The friction factor  $C_f$  for all periodic orbits. While  $C_f$  has maxima at roughly the same points as  $E_{cf}$ , the symbolic dynamics can not be recognized.

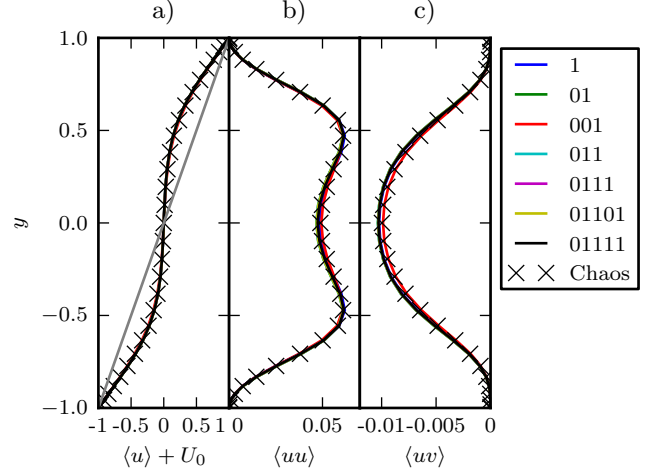


FIG. 10. Averaged quantities of the periodic orbits (lines) and a chaotic trajectory (crosses) as a function of  $y$ . (a) Averaged downstream velocity (b) Fluctuations in the downstream component  $\langle uu \rangle$  (c) Average of  $\langle uv \rangle$ .

where

$$E = \frac{1}{V} \int_V \frac{1}{2} (\vec{u} + \vec{U}_0)^2 dV,$$

$$D = \frac{1}{V} \int_V (\vec{\nabla} \times (\vec{u} + \vec{U}_0))^2 dV,$$

$$I = 1 + \frac{1}{2A} \int_A \left( \frac{\partial u}{\partial y} \Big|_{y=1} + \frac{\partial u}{\partial y} \Big|_{y=-1} \right).$$

In a plot of  $I$  vs.  $D$ , fixed points must lie on the diagonal  $I = D$ . For periodic orbits and also for the non-periodic chaotic motions, the center, defined as time-averages of  $I$  and  $D$ , will also lie on the diagonal. In figure 11 we present all periodic orbits and a chaotic trajectory. The points corresponding to the maxima of  $E_{cf}$  are marked with circles for symbol 0 and squares for 1, the diamond shaped symbol in the lower left corner marks LB. There are three points noteworthy in this figure: first, the symbols are clearly separated and a partition could be based on the location of a maximum in that representation. Second, the periodic orbits capture all of the qualitative features and loops of the chaotic trajectory. And third, one sees that the chaotic trajectory in the background is about to touch LB, the event that will trigger the crisis.

## V. FINAL REMARKS

The detection of periodic orbits in this system was certainly assisted by the fact that the flows studied here were confined to a small domain, restricted by a discrete shift and reflect symmetry, and also analyzed at



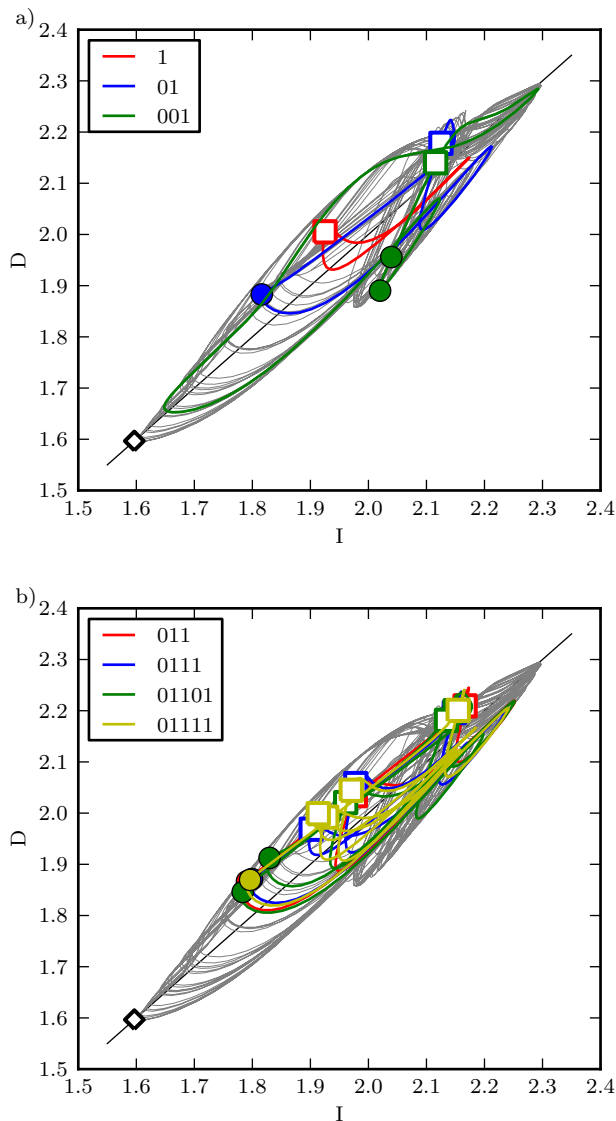


FIG. 11. The periodic orbits in the input-dissipation plane. In the background a chaotic trajectory is plotted in gray. The maxima of  $E_{cf}$  along the orbits are indicated with circles for symbol 0 and open squares for 1. In this plots, the regions of the different symbols do not overlap. It is interesting to notice that the only two symbols below the diagonal belong to the orbit  $\overline{001}$ .

a low Reynolds number. In this sense, it is similar to the study of fluctuations in the Kuramoto-Shivashinsky equation [32]. Nevertheless, the reduction to a symbolic dynamics compatible with a unimodal one-dimensional map and the association of the orbits to the universal Metropolis -Stein-Stein sequence shows that also this high-dimensional system follows the universal dynamics identified in low-dimensional systems. This raises the hope that bifurcation analyses and periodic orbits can also be identified and used in other systems, such as pipe flows or plane Poiseuille flow. The ultimate goal, however, is to analyze not only chaotic but also some turbulent flows in terms of periodic orbits, as suggested e.g. in [44].

## ACKNOWLEDGEMENTS

We would like to thank John F Gibson for developing and providing access to his code *channelflow*, on which the calculations presented here are based, and Normal Lebovitz and Tobias M Schneider for helpful discussions. This work was supported in part by the German Research Foundation within Forschergruppe 1182.

- 
- [1] J. P. Eckmann. Roads to turbulence in dissipative dynamical systems. *Rev. Mod. Phys.*, 53:643–654, Oct 1981.
  - [2] Edward Ott. Strange attractors and chaotic motions of dynamical systems. *Rev. Mod. Phys.*, 53:655–671, Oct 1981.
  - [3] Bruno Eckhardt, Tobias M. Schneider, Bjorn Hof, and Jerry Westerweel. Turbulence transition in pipe flow. *Annual Review of Fluid Mechanics*, 39(1):447–468, 2007.
  - [4] Bruno Eckhardt. Turbulence transition in pipe flow: some open questions. *Nonlinearity*, 21(1):T1, 2008.
  - [5] P Cvitanovic and B Eckhardt. Periodic orbit expansions for classical smooth flows. *Journal of Physics A: Mathematical and General*, 24(5):L237, 1991.
  - [6] C. David Andereck, S. S. Liu, and Harry L. Swinney. Flow regimes in a circular Couette system with independently rotating cylinders. *Journal of Fluid Mechanics*, 164:155–183, 1986.
  - [7] E.L. Koschmieder. *Bénard Cells and Taylor Vortices*. Cambridge Monographs on Mechanics and Applied Mathematics. Cambridge University Press, 1993.

- [8] Maurer, J. and Libchaber, A. Rayleigh-bénard experiment in liquid helium ; frequency locking and the onset of turbulence. *J. Physique Lett.*, 40(16):419–423, 1979.
- [9] J. Stavans, F. Heslot, and A. Libchaber. Fixed winding number and the quasiperiodic route to chaos in a convective fluid. *Phys. Rev. Lett.*, 55:1239–1239, Sep 1985.
- [10] F H Busse. Non-linear properties of thermal convection. *Reports on Progress in Physics*, 41(12):1929, 1978.
- [11] M. C. Cross and P. C. Hohenberg. Pattern formation outside of equilibrium. *Rev. Mod. Phys.*, 65:851–1112, Jul 1993.
- [12] M. Nagata. Three-dimensional finite-amplitude solutions in plane Couette flow: bifurcation from infinity. *Journal of Fluid Mechanics*, 217:519–527, 1990.
- [13] H. K. Moffatt. Fixed points of turbulent dynamical systems and suppression of nonlinearity Comment 1. In J. L. Lumley, editor, *Whither Turbulence? Turbulence at the Crossroads*, volume 357 of *Lecture Notes in Physics*, Berlin Springer Verlag, pages 250–257, 1990.
- [14] Javier Jiménez and Parviz Moin. The minimal flow unit in near-wall turbulence. *Journal of Fluid Mechanics*, 225:213–240, 1991.
- [15] James M. Hamilton, John Kim, and Fabian Waleffe. Regeneration mechanisms of near-wall turbulence structures. *Journal of Fluid Mechanics*, 287:317–348, 1995.
- [16] Fabian Waleffe. Hydrodynamic stability and turbulence: beyond transients to a self-sustaining process. *Stud. Appl. Math.*, 95:319–343, 1995.
- [17] W. Schoppa and F. Hussain. Coherent structure generation in near-wall turbulence. *Journal of Fluid Mechanics*, 453:57–108, 2002.
- [18] M. Lagha and P. Manneville. Modeling transitional plane Couette flow. *The European Physical Journal B - Condensed Matter and Complex Systems*, 58:433–447, 2007. 10.1140/epjb/e2007-00243-y.
- [19] Nadine Aubry, Philip Holmes, John L. Lumley, and Emily Stone. The dynamics of coherent structures in the wall region of a turbulent boundary layer. *Journal of Fluid Mechanics*, 192:115–173, 1988.
- [20] T.R. Smith, J. Moehlis, and P. Holmes. Heteroclinic cycles and periodic orbits for the  $O(2)$ -equivariant 0:1:2 mode interaction. *Physica D*, 211:347–376, 2005.
- [21] Holger Faisst and Bruno Eckhardt. Transition from the Couette-Taylor system to the plane Couette system. *Phys. Rev. E*, 61:7227–7230, Jun 2000.
- [22] Holger Faisst and Bruno Eckhardt. Traveling waves in pipe flow. *Phys. Rev. Lett.*, 91(22):224502, Nov 2003.
- [23] Björn Hof, Casimir W. H. van Doorne, Jerry Westerweel, Frans T. M. Nieuwstadt, Holger Faisst, Bruno Eckhardt, Hakan Wedin, Richard R. Kerswell, and Fabian Waleffe. Experimental observation of nonlinear traveling waves in turbulent pipe flow. *Science*, 305(5690):1594–1598, 2004.
- [24] Tobias M. Schneider, Bruno Eckhardt, and Jürgen Vollmer. Statistical analysis of coherent structures in transitional pipe flow. *Phys. Rev. E*, 75:066313, Jun 2007.
- [25] YC Lai and T Tel. *Transient Chaos*. Springer, 2011.
- [26] Bjorn Hof, Jerry Westerweel, Tobias M. Schneider, and Bruno Eckhardt. Finite lifetime of turbulence in shear flows. *Nature*, 443:59–62, 2006.
- [27] Tobias M. Schneider and Bruno Eckhardt. Lifetime statistics in transitional pipe flow. *Phys. Rev. E*, 78:046310, Oct 2008.
- [28] R. M. Clever and F. H. Busse. Tertiary and quaternary solutions for plane Couette flow. *Journal of Fluid Mechanics*, 344:137–153, 1997.
- [29] F. Mellibovsky and B. Eckhardt. Takens-Bogdanov bifurcation of travelling-wave solutions in pipe flow. *Journal of Fluid Mechanics*, 670:96–129, 2011.
- [30] F. Mellibovsky and B. Eckhardt. From travelling waves to mild chaos: a supercritical bifurcation cascade in pipe flow. *submitted*, 2012.
- [31] Bruno Eckhardt and Gerolf Ott. Periodic orbit analysis of the lorenz attractor. *Zeitschrift für Physik B Condensed Matter*, 93:259–266, 1994. 10.1007/BF01316970.
- [32] F Christiansen, P Cvitanovic, and V Putkaradze. Spatiotemporal chaos in terms of unstable recurrent patterns. *Nonlinearity*, 10(1):55, 1997.
- [33] Genta Kawahara and Shigeo Kida. Periodic motion embedded in plane couette turbulence: regeneration cycle and burst. *Journal of Fluid Mechanics*, 449:291–300, 2001.
- [34] John F. Gibson. Channelflow website. [www.channelflow.org](http://www.channelflow.org), 2011.
- [35] P.G. Drazin and W.H. Reid. *Hydrodynamic Stability*. Cambridge Mathematical Library, 2. edition, 2004.
- [36] Norman R Lebovitz. Shear-flow transition: the basin boundary. *Nonlinearity*, 22(11):2645, 2009.
- [37] Norman R. Lebovitz. Boundary collapse in models of shear-flow transition. *Communications in Nonlinear Science and Numerical Simulation*, 17(5):2095–2100, 2012.
- [38] Lennaert van Veen and Genta Kawahara. Homoclinic tangle on the edge of shear turbulence. *Phys. Rev. Lett.*, 107:114501, Sep 2011.
- [39] Jürgen Vollmer, Tobias M. Schneider, and Bruno Eckhardt. Basin boundary, edge of chaos and edge state in a two-dimensional model. *New Journal of Physics*, 11(1):013040, 2009.
- [40] Celso Grebogi, Edward Ott, and James A. Yorke. Crises, sudden changes in chaotic attractors, and transient chaos. *Physica D: Nonlinear Phenomena*, 7(1–3):181–200, 1983.
- [41] D. Viswanath. Recurrent motions within plane couette turbulence. *Journal of Fluid Mechanics*, 580:339–358, 2007.
- [42] N Metropolis, M.L Stein, and P.R Stein. On finite limit sets for transformations on the unit interval. *Journal of Combinatorial Theory, Series A*, 15(1):25–44, 1973.
- [43] J. F. Gibson, J. Halcrow, and P. Cvitanović. Visualizing the geometry of state space in plane Couette flow. *Journal of Fluid Mechanics*, 611:107–130, 2008.
- [44] Lennaert van Veen, Shigeo Kida, and Genta Kawahara. Periodic motion representing isotropic turbulence. *Fluid Dynamics Research*, 38(1):19–46, 2006.